Coupled nonhomogeneous flows and flow-enhanced concentration fluctuations during startup shear of entangled polymer solutions

Michael C. Burroughs [1], Abhishek M. Shetty [2], L. Gary Leal [1], and Matthew E. Helgeson [1,*]

[1]*Department of Chemical Engineering, University of California, Santa Barbara, Santa Barbara, California 93106, USA*

[2]*Anton Paar USA Inc., Ashland, Virginia 23005, USA*

(Received 1 October 2019; revised manuscript received 23 January 2020; accepted 31 March 2020; published 27 April 2020)

The flow behavior of entangled polymer solutions in simple shear flow is often assumed to be uniform, both in terms of the velocity gradient and polymer concentration. However, there is growing evidence of nonuniform "banded" transient or steady state flows of entangled polymer solutions. The present work considers a distinct phenomenon, whereby transient banding is concomitant with the presence of local shear-enhanced concentration fluctuations. Experimental observations are made using combined rheological measurements with simultaneous particle tracking velocimetry and microscopy (rheomicroscopy) during startup shear in Taylor-Couette flow of entangled polymer solutions of polystyrene in a marginal solvent, dioctyl phthalate, at various entanglement numbers (Z). At high Z, the flow develops transient, nonhomogeneous "banded" velocity profiles over a wide range of imposed shear rates that are inverted from those expected for Taylor-Couette flow, which then relax to a nearly uniform shear rate at steady state. Rheomicroscopy reveals that these transient banded states are accompanied by strong shear-enhanced concentration fluctuations localized to the region of lowest local shear rate. We hypothesize that such finite-amplitude concentration fluctuations lead to increased dissipation that contributes a higher local "effective" fluid viscosity that, in turn, could produce the observed flow nonuniformity. In spite of the nonuniformity of the flow and the concentration fluctuations, the measured apparent rheology of the fluids is in qualitative agreement with both prior experimental studies and model predictions based on a Rolie-Poly model under the assumption that the fluid remains homogeneous, suggesting that this behavior is only observable through spatially resolved measurements of fluid flow and concentration.

DOI: 10.1103/PhysRevFluids.5.043301

I. INTRODUCTION

A long-standing goal of polymer physics is to develop a microscopically based constitutive theory to model how the microstructure of entangled polymers under flow results in the measured macroscopic stresses. To date, tube-based models, derived from the Doi-Edwards constitutive equation [1] constructed from the reptation idea of de Gennes [2], have been the most successful in achieving this goal. In part, this success is due to the identification and inclusion of a number of relaxation mechanisms in addition to reptation [contour length fluctuations (CLF), thermal constraint release (TCR), convective constraint release (CCR), and relaxation of chain stretch] [3–7]. Although comparison of these models with linear viscoelastic data has shown remarkable agreement, accurate prediction of nonlinear rheological properties has proven to be more challenging. One possible issue

*Corresponding author: helgeson@ucsb.edu

could be the description of chain dynamics in the nonlinear regime, which has received intense theoretical investigation [3,5,6,8,9]. Another possible issue is the assumption, made in nearly all studies, that the fluids (and viscoelastic flows they give rise to) remain homogeneous. In the case of polymer solutions, this means that the polymer concentration remains uniform mesoscopically and across macroscopic length scales.

Contrary to this assumption, some polymer-solvent combinations exhibit shear-enhanced concentration fluctuations as indicated by strong fluctuations in measurable optical properties [10–16]. In particular, solutions of polystyrene (PS) in dioctyl phthalate (DOP) have been examined extensively for understanding the occurrence of shear-enhanced concentration fluctuations due to the temperature-dependent solvent quality and large refractive index contrast between PS and DOP [10–13,15–26]. Although fluid velocities have not typically been measured, it has generally been assumed that these concentration fluctuations are not accompanied by any measurable change in the macroscopic flow. Another possibility, presumably at higher shear rates, is that the same physics responsible for concentration fluctuations may lead to shear-induced demixing on a macroscopic scale, and thus to "banding" of the macroscopic concentration profiles as predicted in recent work [27–32]. When this shear-induced "banding" of the polymer concentration profile occurs, it is clear that there must be corresponding changes in the macroscale flow. For planar shear flow, the velocity profile is predicted to have a banded shape in the absence of a constitutive instability. To date, however, the simultaneous occurrence of banded concentration and velocity profiles has yet to be demonstrated experimentally [29].

Recently, there have been some reported velocimetry experiments that are inferred to represent shear banding [4,33–39], either as a transient during startup of shear, or as steady state profiles, in both cone-and-plate and Couette devices. Unlike other fluids, it is currently believed that banding in polymers is not due to constitutive instability [4]. However, most of these studies lacked the spatial resolution to differentiate shear banding from other effects. One possibility in Couette flow is that shear thinning can enhance the intrinsic curvature of the velocity profiles so that they can mistakenly be identified as shear banding [40]. It has also been suggested that these nonhomogeneous flows may be a consequence of edge fracture and/or slip [41–44]. This may well be true in some or even many cases, but is also noteworthy that none of the prior studies have included any measurements of the concentration profiles.

When flow inhomogeneity is observed in commonly used rotational rheometric flows, it usually exists with the high shear rate region nearest the moving boundary where the shear stress is largest [45]. Specifically, in Taylor-Couette devices, there is a dimensionless curvature of the geometry (q) that depends on the ratio of the gap width ($R_0 - R_i$) to inner cylinder radius (R_i), ($q = \frac{R_0 - R_i}{R_i}$), which is accompanied by a similar gradient in shear stress. Correspondingly, in a polymer solution, the high shear rate region is usually observed near the rotating inner cylinder. However, in rare cases, reversed profiles have been reported for cone-and-plate flow [4,35,46], with the high shear rate region near the stationary boundary. Surprisingly, when the transient shear stress is measured during startup in the latter cases, it agrees qualitatively with expectations for an entangled polymer solution, with a transient overshoot in the measured shear stress exhibiting all of the expected behavior (such as the dependence on the time to the maximum shear stress having the usual dependence on shear rate). One observation common to all systems in startup of shear flow is that the onset of nonhomogeneous velocity profiles occurs shortly after the shear stress maximum.

To date, as noted earlier, the role of shear-enhanced concentration fluctuations in entangled polymer solutions has been neglected in experimental studies of nonhomogeneous flows. Specifically, in experimental studies of shear-enhanced concentration fluctuations, the velocity profiles were not measured. Nevertheless, it has been shown, both theoretically [14,47–49] and experimentally [11–13,15,16,21,23,24,50,51], that shear flow can amplify and orient concentration fluctuations in entangled polymer solutions. Polymer solutions near an equilibrium phase boundary are particularly susceptible to such fluctuations due to the approach toward vanishing osmotic compressibility near the critical point.

Experimentally, concentration heterogeneities can be detected using *in situ* microscopy and light scattering [52], and possess a characteristic length ($l_c = \sqrt{D\tau_d}$), which depends on the longest relaxation time (τ_d) and the cooperative diffusivity (D), that corresponds to the length scale at which the rates of stress relaxation and polymer diffusion are equal [48]. In high molecular weight, semidilute entangled polymers l_c can be large relative to the polymer radius of gyration. Even though it is generally believed that these finite-amplitude concentration fluctuations occur at a local scale, it is foreseeable that sufficiently long-range concentration fluctuations (or gradients thereof) may alter the flow uniformity of entangled polymer solutions. However, this possibility has not received detailed study [53].

In the present work, we report combined rheometry and velocimetry measurements on the flow of entangled polystyrene (PS) in dioctyl phthalate (DOP) solutions in a Taylor-Couette device modified to eliminate edge fracture over an extended shear rate range. The goal is to better understand the possible coupling between shear-enhanced concentration fluctuations and the potential for nonhomogeneous flows of entangled polymer solutions. These measurements confirm that nonhomogeneous flow can occur as a transient in highly entangled polymer solutions, where the velocity profile develops two regions of different shear rate shortly after the startup of shear flow. Unexpectedly, however, the PS-DOP system at high concentrations (large Z) shows banded profiles that have the inverse configuration to that usually expected for Taylor-Couette flow, with the high shear rate region nearest the stationary outer cylinder. To our knowledge, such an inverted profile cannot be predicted with any existing constitutive model for homogeneous polymer solutions. Corresponding *in situ* rheomicroscopy measurements reveal that pronounced flow-enhanced concentration fluctuations transiently appear, evolve, and subside as the flow evolves toward steady state. Furthermore, the region of strong flow-enhanced concentration heterogeneities is observed to coincide with the low shear rate portion of the velocity profiles adjacent to the moving cylinder (where the shear stress is largest). We suspect that increased dissipation, and correspondingly an increased effective viscosity, of the fluid due to finite-amplitude concentration fluctuations may provide a possible explanation for this previously unreported behavior.

II. MATERIALS AND METHODS

Polystyrene (PS) with reported molecular weights of 3.84×10^6 and 8.42×10^6 g/mol and polydispersity indices of 1.04 and 1.17, respectively, was purchased from Tosoh Biosciences, LLC. Dioctyl phthalate (DOP) (CAS No. 117-81-7, $\geqslant$99.5%) was purchased from Sigma-Aldrich. Glass tracer particles with a diameter of $\sim10\,\mu$m were donated by TSI Incorporated. All materials were used as supplied without further purification.

Highly entangled PS-DOP solutions were prepared by adding DOP to desired amounts of PS and tracer particles. The labeling convention adopted for the PS-DOP solutions was based on the concentration and molecular weight of PS [i.e., 10 wt% PS(8.42M)-DOP corresponds to a solution that is 10 wt% PS with a molecular weight of 8.42×10^6 g/mol]. The number of entanglements (Z) per chain was estimated by

$$Z = \frac{M_w}{M_e}\phi^{\alpha}, \tag{1}$$

where M_w is the weight-average molecular weight, M_e is the entanglement molecular weight in the melt (13 500 g/mol for PS), and the dilution exponent α was assumed to be 1.2 to directly compare with previous work on shear banding in polymer solutions where this same exponent was used [33,37,41,42]. For 10-g samples, ~50 ml of toluene was added as a cosolvent to aid in dissolution. The samples were mixed for several days on a stir plate at a temperature of 50 °C. Once the polymer was completely dissolved, the toluene was evaporated in a fume hood until the samples became too viscous to mix with a stir bar. The remaining toluene was removed by placing the samples in a vacuum oven (~–350 mm Hg) until the residual toluene fell below 0.1 wt% of the total sample as determined gravimetrically. The final concentration of tracer particles was 300–500 ppm.

All linear viscoelasticity and particle tracking measurements were conducted on an Anton Paar MCR-300 stress-controlled rheometer described previously [54]. The rheometer was equipped with a Taylor-Couette flow cell comprising a transparent quartz cup, where the temperature was controlled by flowing water from a water bath through an annulus in the quartz. The quartz cup was 22 mm deep and the inner cylinder (bob), with an anodized aluminum surface, was 16 mm tall. The bob had a diameter of 34 mm and the inner diameter of the cup was 35 mm, yielding a gap size of 0.5 mm and a curvature $q = 0.029$. The diameter of the bob was selected to minimize the effect of curvature on the experiments.

The transparent quartz cup allowed for particle tracking velocimetry (PTV) measurements to be conducted simultaneously with rheological experiments as described in detail elsewhere [54]. Briefly, plano-convex and concave lenses were used to transform the light from a laser head into a two-dimensional (2D) sheet. The laser sheet illuminated tracer particles from the side of the flow cell in the velocity-velocity gradient plane within the geometry gap. A camera positioned underneath the Taylor-Couette flow cell captured images at a fixed frame rate depending on the applied shear rate. The tracer particles were identified, and their displacements between subsequent image pairs calculated, using an image processing algorithm [55]. In all PTV measurements, the illuminated plane was roughly 3 mm above the bottom edge of the Taylor-Couette bob. We observe no changes in the measured velocity profiles upon varying the position of the illuminated plane from 1 mm from the bottom edge of the bob to its midplane. This result, as well as visual observation, confirms the absence of curvature-induced elastic instability as predicted by Larson *et al.* [56] to occur in Taylor-Couette flows at a sufficiently large Weissenberg number. This absence of elastic instability in our experiments is in agreement with the instability criterion proposed by Larson *et al.* [56]; for the curvature of $q = 0.029$, this criterion predicts that the critical Weissenberg number for the Taylor-Couette flow cell is approximately 35, which is much higher than the applied Wi used in this study.

The degree of shear-enhanced concentration fluctuations was controlled by varying the temperature of the PS-DOP solutions. PS-DOP has a well-characterized theta temperature of 22 °C. We employed a higher temperature of 50 °C for PTV measurements with the higher concentration PS solutions as a means to control the magnitude of turbidity, which was too strong for particle tracking measurements when these samples were sheared near the theta temperature.

Bright field rheomicroscopy measurements were performed on an Anton Paar MCR-702 stress-controlled rheometer. The rheometer was fitted with a transparent quartz cup of similar dimensions as used in the rheo-PTV measurements as well as the same anodized aluminum bob. A white LED light source was positioned above the Taylor-Couette cell to illuminate the fluid. A $10\times/\mathrm{NA} = 0.28$ objective (Mitutoyo, Japan) with a charge-coupled device (CCD) camera (1.4 megapixel mini enclosed color camera, Model No. Lm165C, Lumenera) was mounted underneath the flow cell to image the fluid in transmission mode. The focal depth of the objective was 3.5 μm. Crossed polarizers were placed above and below the flow cell at 90° relative polarization in order to minimize noise in the microscopy images. A digital Fourier band pass filter for structures between 0.49 and 1.95 $\mu\mathrm{m}^{-1}$ was applied to each captured image. This range was believed to capture the length scale of actual shear-induced structures in the fluid based upon the optical heterogeneities observed in the raw microscopy images.

To minimize the effect of edge fracture, a stainless-steel lid was machined and placed on top of the fluid. The sample is loaded into the quartz cup in excess so that it comes in contact with the lid after the bob is fully submerged, yielding geometrically symmetric boundary conditions on the top and bottom of the Taylor-Couette flow cell. We expect that any secondary flow resulting from the boundaries will only be significant over distances comparable to the gap width (500 μm). The results of this paper are found to be invariant to the vertical location of the PTV measurement as measured at several positions from near the bottom edge of the bob to the midplane. In addition, the results reported are the same over observable timescales with and without the stainless-steel lid; therefore, we conclude that the presence of a lid on top of the fluid only serves to extend the lifetime of a reliable rheological measurement.

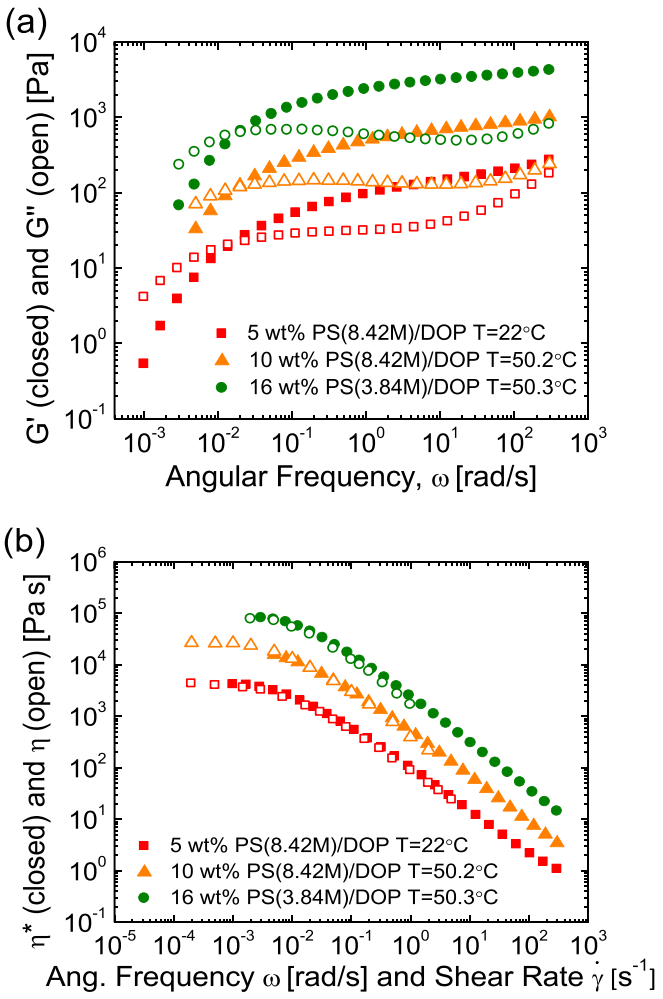

FIG. 1. (a) Linear viscoelastic frequency sweeps for three entangled PS-DOP solutions. Measurements were conducted at a strain = 1%, and (b) verification of Cox-Merz rule for shear rates employed in this study.

Samples were loaded into the quartz cup by spatula at an elevated temperature to reduce the time needed for the polymer solutions to equilibrate. Once the air bubbles introduced by loading were eliminated, the bob was slowly lowered into the sample to avoid excessive normal forces.

III. RESULTS AND DISCUSSION

A. Linear rheological characterization of polystyrene solutions

Three solutions of entangled polystyrene (PS) in dioctyl phthalate (DOP) were prepared, with entanglement numbers (Z) ranging from 16 to 36. The linear viscoelastic response of each PS-DOP solution is shown in Fig. 1(a). For each solution, the frequency of the crossover of the storage modulus (G') and the loss modulus (G'') is separated from the local minimum in G'' (which appears at higher frequency) by approximately three decades, indicating significant entanglement. The relaxation time for reptation (τ_d) is the inverse of the frequency at which G' and G'' cross over, determined by linear interpolation. The plateau modulus (G_N^0) is defined as the value of G' at the frequency where G'' exhibits a local minimum.

TABLE I. Viscoelastic solution properties determined from rheological measurements. The Rouse time was calculated from the measured τ_d (s) and the relation $\frac{\tau_d}{\tau_R} = 3Z$.

Solution	Entanglements per chain, Z	Reptation time τ_d (s)	Plateau modulus, G_N^0 (Pa)	Zero-shear viscosity η_0 (Pa s)	Recoverable compliance, J_e^0 (Pa^{-1})	Rouse time, τ_R (s)
5 wt% PS(8.42M)-DOP	16	60.9	126	4.29×10^3	9.78×10^{-3}	1.27
10 wt% PS(8.42M)-DOP	36	55.5	701	2.66×10^4	1.78×10^{-3}	0.51
16 wt% PS(3.84M)-DOP	30	51.4	3.29×10^3	7.77×10^4	4.41×10^{-4}	0.57

Complex viscosities (η^*) were extracted from linear viscoelastic frequency sweeps. Shear viscosities (η) were determined by averaging the measured viscosity at long times following a rapid ramp of the inner cylinder from rest to the target wall velocity necessary to achieve a specified shear rate (assuming homogeneous shear flow). The Cox-Merz rule is satisfied for each solution, demonstrated by a simultaneous plot of $\eta^*(\omega)$ and $\eta(\dot\gamma)$, Fig. 1(b). Table I summarizes the rheological properties for each solution. All three solutions show evidence of a zero-shear viscosity given by the plateau in viscosity at low shear rates and shear thinning above an approximate shear rate given by τ_d^{-1}. The degree of shear thinning, characterized by a dependence of $\dot\gamma^n$ of $-0.89 \leqslant n \leqslant -0.81$, agrees with previous reports on entangled polymer solutions [7,9].

B. Comparisons of steady state experimental data to the homogeneous Rolie-Poly model

To confirm that the fluids in this study exhibit the expected rheological behavior across the range of conditions investigated, the variations in measured steady state shear stresses for the three different entangled solutions with varying imposed nominal Wi_{app} where

$$Wi_{\text{app}} = \tau_d \dot\gamma \tag{2}$$

were compared to predictions from the homogeneous Rolie-Poly (RP) constitutive model (Fig. 2). Details of the homogeneous (RP) model are included in the Supplemental Material [57]. For comparison, the shear stress ($\sigma_{r\theta}$) was determined from the measured torque of the rheometer and the recoverable compliance (J_e^0) was calculated from the zero-frequency extrapolation of the linear viscoelastic data in Fig. 1(a), given by

$$\lim_{\omega\to 0} \frac{G'(\omega)}{[G'(\omega)^2 + G''(\omega)^2]}. \tag{3}$$

The shear rate used to determine Wi was based on the nominal imposed shear rate (Wi_{app}), which assumes a linear velocity profile. In the linear flow regime ($Wi < 1$), Newtonian behavior is predicted and observed for all three entangled solutions, as reflected in a linear slope of $\sigma_{r\theta}J_e^0$ versus Wi. For nonlinear flows ($Wi > 1$), all solutions exhibit a weaker dependence of $\sigma_{r\theta}J_e^0$ versus Wi. The broader transition from Newtonian behavior to a weak plateau in $\sigma_{r\theta}J_e^0$ relative to the (RP) model predictions could result from the polydispersity of the polystyrene used in experiments, leading to a distribution of relaxation times that is neglected by the single-mode RP model.

Otherwise, for steady state flows, the homogeneous RP model appears to accurately describe both the linear and nonlinear shear rheology of the three entangled solutions. Both the model and measured shear stress values are strictly increasing (monotonic) for all applied Wi, which precludes the possibility of flow instability arising from a nonmonotonic flow curve.

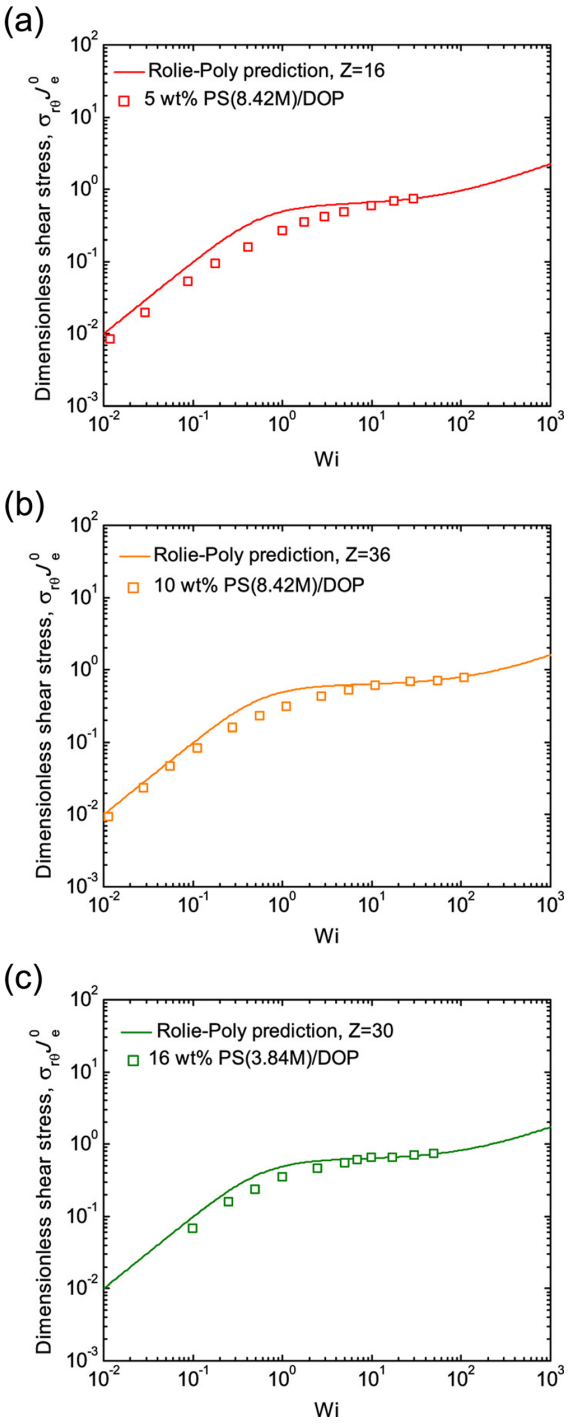

FIG. 2. Rolie-Poly model flow curve predictions (lines) and measured steady state shear stresses (symbols) for (a) 5 wt% PS(8.42M)-DOP, (b) 10 wt% PS(8.42M)-DOP, and (c) 16 wt% PS(3.84M)-DOP.

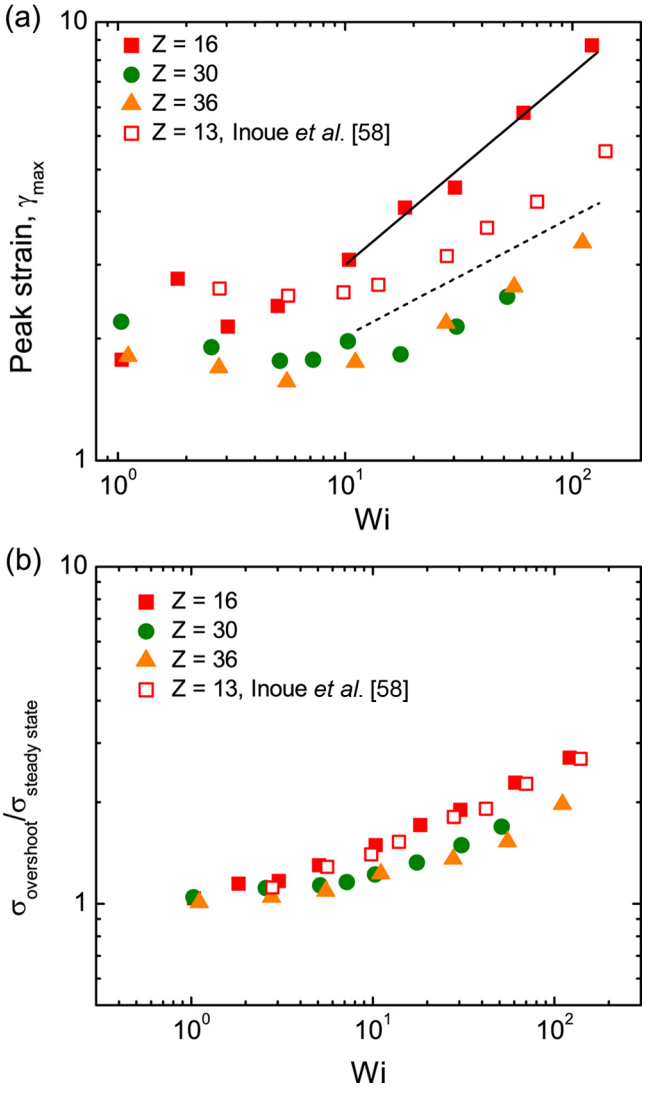

FIG. 3. (a) Wi dependence of the peak strain (γ_{max}, strain at which the shear stress exhibits an overshoot) following startup shear where the solid and dashed lines indicate power law slopes of 0.45 and 0.28, respectively, and (b) the ratio of the maximum shear stress to the shear stress at steady state ($\sigma_{overshoot}/\sigma_{steady\ state}$) for varying Wi.

C. Comparison of transient experimental data to previous work

The transient shear stress results were found to agree with previously reported startup shear experiments on entangled PS-DOP solutions, albeit with fewer entanglements per chain ($Z \sim 13$) [58]. Figure 3 illustrates the influence of applied Wi on the transient stress response for the three entangled PS-DOP solutions, as well as previously reported results for an entangled PS-DOP solution [58]. More specifically, the strain at which the shear stress overshoot occurs following the startup of flow increases above $Wi \sim 10$ in all solutions [Fig. 3(a)]. For $Wi \leqslant 10$ the strain at the shear stress overshoot is around 2, in agreement with past reports.

The ratio of the shear stress at the overshoot to the steady state value for varying Wi also agrees quantitatively with literature values [58] for $Z = 16$ [Fig. 3(b)]. However, the solutions with $Z = 30$

and 36 have lower values of the ratio $\sigma_{\text{overshoot}}/\sigma_{\text{steady state}}$ for high Wi compared to the solutions with lower Z. The difference between the high Wi values of $\sigma_{\text{overshoot}}/\sigma_{\text{steady state}}$ in PS-DOP solutions with high and low entanglements could be due to more chain stretching in the less entangled solutions relative to the highly entangled solutions (i.e., longer Rouse relaxation times). In summary, aside from a quantitative difference in the ratio $\sigma_{\text{overshoot}}/\sigma_{\text{steady state}}$ with Wi for the solutions with higher levels of entanglement, the measured rheology of the PS-DOP solutions agrees qualitatively and quantitatively with what has been reported in the literature previously, and there is no evidence that can be discerned from the shear stress data (or the homogeneous RP model predictions) that potentially suggests a departure from homogeneous flow of the entangled polymer solutions in the startup of shear flow.

D. Observation of nonhomogeneous flow in highly entangled solutions

To investigate the kinematic response of entangled polymer solutions subjected to startup of steady shear flow, rheo-PTV measurements were conducted to obtain the velocity profile and shear stress at numerous nominal imposed Wi to be quantified simultaneously. In a Taylor-Couette geometry, curvature or "bowing" in the measured velocity profiles is expected, resulting from the inherent shear stress gradient for flow between concentric cylinders ($\sigma_{r\theta} \sim \frac{1}{r^2}$), with the highest shear rate at the inner (moving) cylinder and lowest at the outer (stationary) cylinder. For shear thinning fluids, this curvature in the measured velocity profile is more pronounced than for a Newtonian fluid, due to the nonlinear dependence of shear stress on shear rate.

There is a strong departure from this expected flow behavior in highly entangled PS-DOP solutions. A representative example is the measured velocity profiles in the range $\frac{t}{\tau_d} = 7-11$ following the startup of shear flow in 10 wt% PS(8.42M)-DOP ($Z = 36$), which are inversely banded for a wide range of Wi_{app} (Fig. 4). Such nonhomogeneous flow profiles are surprising since steady shearing for $10\,\tau_d$ is commonly believed to be sufficient time to achieve steady state flow, as determined by the measured shear stress. Nonzero velocities at $r/H = 1.0$ are also observed and are presumably due to wall slip at the stationary quartz boundary. Attempts to eliminate wall slip by applying a plastic film to the quartz boundary were found to complicate the measurements as the fluid would inevitably delaminate the film from the quartz surface, yielding a nonuniform gap length around the Taylor-Couette flow cell. The presence of wall slip could certainly amplify the magnitude of the observed inversely bowed velocity profiles, but transient changes in the velocity profiles are observed even after the slip velocity has reached a steady state. For $Wi_{\text{app}} \geqslant 5.55$, the velocity profiles appear to have two distinct regions of differing shear rate, where the high shear rate region is adjacent to the stationary boundary and the low shear rate region is next to the moving boundary. This disagrees with the expectation for nonhomogeneous flows that the highest shear rate occurs in the region of highest shear stress (i.e., the moving boundary). To investigate the flow kinematics of entangled polymer solutions further, we studied the transient development of the inversely bowed velocity profiles and consider a phenomenon that could potentially explain the observation of nonhomogeneous flow.

E. Transient development of flows during startup of steady shear

1. Moderately entangled solution ($Z = 16$)

For $Wi_{\text{app}} > 1$, an overshoot in the transient shear stress occurs in entangled PS-DOP solutions [Fig. 5(a)]. The initial shear stress response in startup of steady shear flow is governed by the elasticity of the fluid. As seen for a moderately entangled ($Z = 16$) solution of 5 wt% PS(8.42M)-DOP in Fig. 5(b), the velocity profile remains linear prior to the overshoot in the shear stress at $\frac{t}{\tau_d} = 0.45$. After the overshoot, the shear stress decreases slowly toward its steady state value, and the velocity profile develops curvature that can be explained by the geometrically imposed stress gradient of the Taylor-Couette geometry. Such a curved velocity profile is stable for the remainder of the experiment, showing no changes for a period spanning $100\tau_d$. For $Z = 16$, the measured

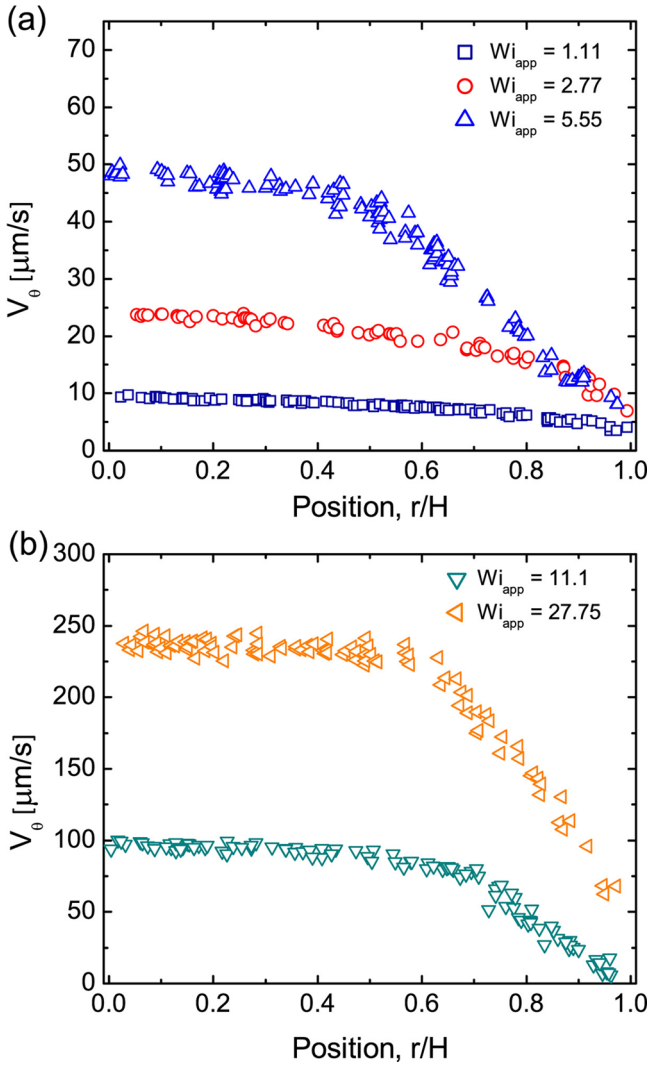

FIG. 4. Velocity profiles for 10 wt% PS(8.42M)-DOP ($Z = 36$) at varying applied Wi for times between $\frac{t}{\tau_d} \sim 7$ and 11 after startup of shear flow.

rheology and flow kinematics thus match expectations from the homogeneous RP model [Fig. 5(b), dotted line]. Thus, when the solution is only moderately entangled ($Z = 16$) the development of both the shear stress and velocity profiles correspond to expectations for a homogeneous fluid in a homogeneous flow. Specifically, the inverted velocity profiles apparent for the more highly entangled solutions (Fig. 4) are not observed when $Z = 16$.

2. Highly entangled solutions ($Z = 30$ and 36)

For $Z = 36$ [Fig. 6(a)], the qualitative response of the measured shear stress following startup of continuous shear flow is similar to that in Fig. 5(a), where a shear stress overshoot occurs shortly after shearing commences, followed by a slow decrease to the steady state shear stress. One noticeable difference in the measured shear stress in Fig. 6(a) is the small second overshoot at long times ($\frac{t}{\tau_d} \sim 30-40$). This second overshoot in the shear stress has been observed in investigations of shear-enhanced concentration fluctuations in entangled polymer solutions and was attributed to

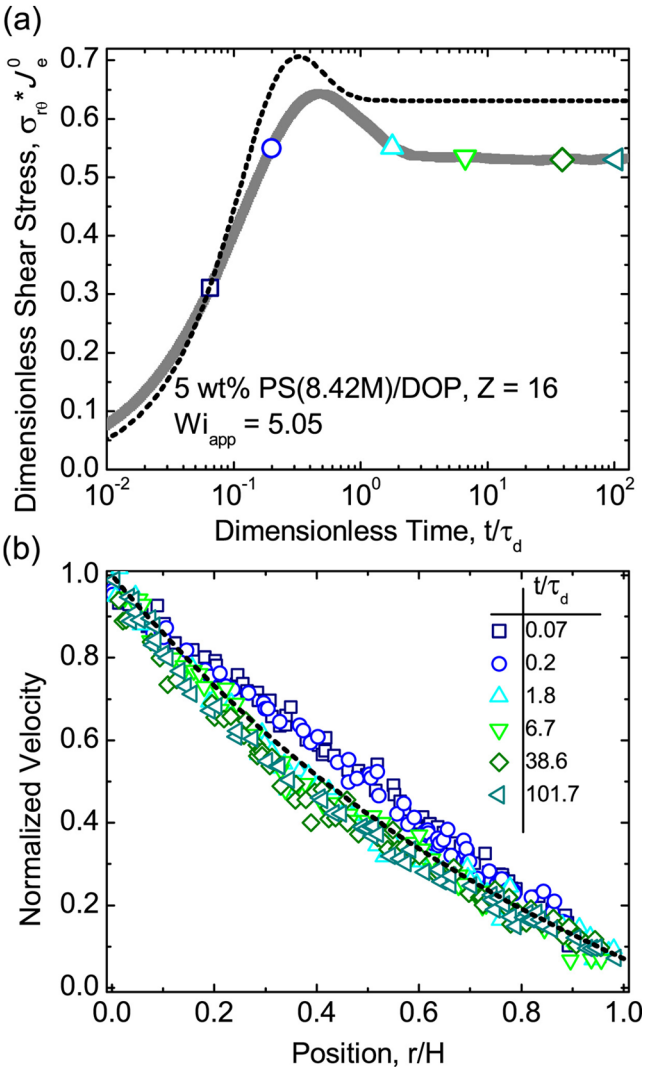

FIG. 5. Transient response of PS-DOP solution with $Z = 16$ to step shear of $Wi = 5.05$ (a) shear stress and (b) velocity profile data. The symbols overlaid on the shear stress response correspond to the time at which the velocity profiles in (b) were measured. Black dashed lines denote the homogeneous Rolie-Poly model prediction for the transient shear stress in (a) and the steady velocity in (b).

the onset of shear-induced demixing [58–61]. The time at which the second overshoot occurs is sensitive to the temperature, polymer molecular weight, polymer concentration, and applied shear rate [60,61].

Despite the agreement in the apparent rheological behavior between the experiments and homogeneous Rolie-Poly model predictions [Fig. 2(c)], the measured transient velocity profiles of the highly entangled solutions show a qualitative departure from the RP model predictions as well as the expectations for a homogeneous fluid. In Fig. 6(b), the velocity profile is initially linear without any curvature following the startup of shear. After the shear stress overshoot, the inversely banded velocity profile develops and reaches a maximum severity (as measured by the difference in shear rate between the two regions) when $\frac{t}{\tau_{d_i}} \sim 1.40$, approximately when the shear stress reaches a local minimum. At longer times, the velocity profile begins to relax to the expected, nearly linear

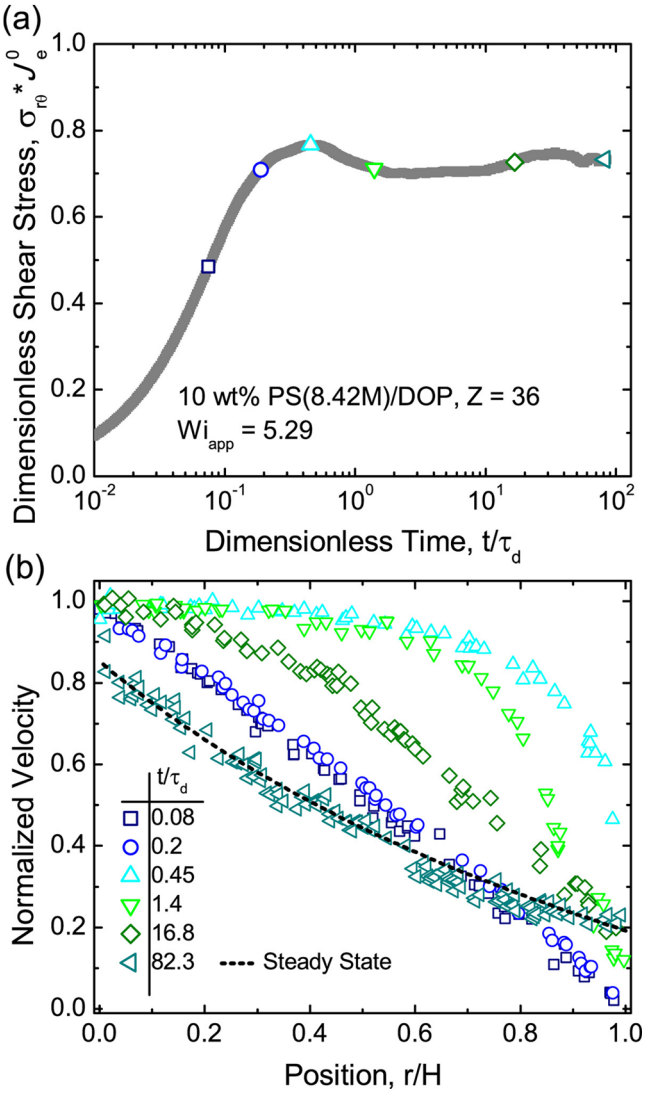

FIG. 6. Transient response of PS-DOP solution with $Z = 36$ to a step shear of $Wi = 5.29$ (a) measured shear stress response and (b) determined velocity profiles for discrete points in time following the startup of flow. Symbols overlaying the measured shear stress in (a) coincide with the point in time of each velocity profile in (b).

form. This relaxation process occurs through a decrease in the difference in shear rate between the two regions, while at the same time the interface between the two regions moves toward the inner moving cylinder and the measured shear stress increases. At very long times following the startup of shear flow, the velocity profile reaches a steady shape where the highest shear rate is next to the moving boundary as expected, and at this point the velocity profile matches what is predicted using the homogeneous RP model after accounting for the appreciable wall slip at both the inner and outer boundaries.

The measured shear stress and velocity profiles for the solution with $Z = 30$ [16 wt% PS(3.84M)-DOP] are qualitatively similar to that for $Z = 36$ [10 wt% PS(8.42M)-DOP] despite the sample having higher concentration, lower polymer molecular weight, and slightly lower degree of

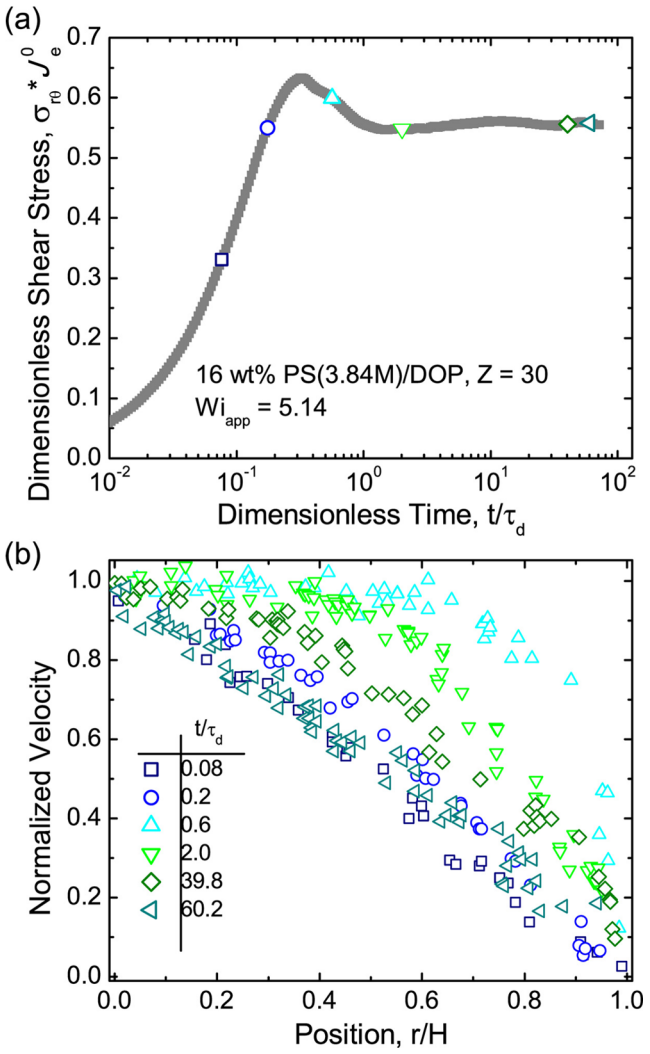

FIG. 7. Transient response of PS-DOP solution with $Z = 30$ to a step shear of $Wi = 5.14$: (a) the measured shear stress and (b) the determined velocity profiles at discrete points in time following the startup of flow.

entanglement (Fig. 7). This suggests that the inversely bowed profiles observed transiently in Figs. 4 and 6(b) are not an artifact of the specific sample or polymer used. The velocity profiles in Fig. 7(b) depart from the expected linear form shortly after the initiation of shear flow. Even in the fluid with $Z = 30$, there is a large difference between the measured shear rate adjacent to the moving and stationary boundaries. Again, at long times the high shear region adjacent to the stationary boundary is no longer present, and the fluid's velocity profile appears nearly linear with some wall slip.

F. Development of localized flow-enhanced concentration heterogeneities in startup shear

A possible explanation for the low shear rate region adjacent to the moving wall is localized shear-enhanced concentration fluctuations. Based on typical values of the diffusivity (D) and reptation time (τ_d) for entangled polymer solutions, the length scale for concentration heterogeneities is estimated to be $O(\mu\text{m})$ due to the competition between diffusion and stress relaxation ($\sqrt{D\tau_d} = l_c$).

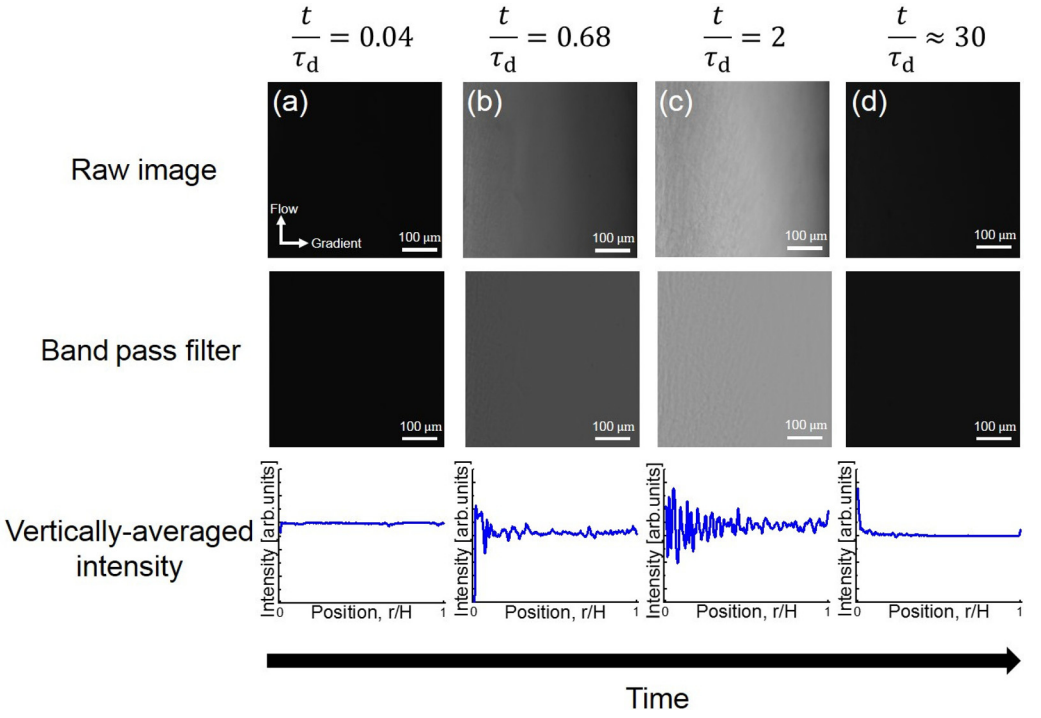

FIG. 8. Rheomicroscopy images showing the development and decay of flow-enhanced concentration fluctuations in 16 wt% PS(3.84M)-DOP at $Wi_{app} = 11.1$: (a) prior to the shear stress overshoot, (b), (c) shortly after the shear stress overshoot, and (c) at long times following the shear stress overshoot when the stress has reached a constant value.

These micron-scale heterogeneities could increase dissipation, and therefore act to increase the effective viscosity of the fluid. More specifically, because the shear-induced enhancement of concentration heterogeneities is sensitive to the local shear stress, a stress gradient (such as encountered in the Taylor-Couette geometry) could consequently produce spatial variations in the concentration fluctuations and therefore the local effective fluid viscosity. For example, if shear-enhanced concentration fluctuations were largest in the region of highest local stress (the inner rotating cylinder), this could increase the effective viscosity by such an amount as to produce the observed low shear rate region near the moving cylinder in our experiments.

To further investigate the presence of such flow-enhanced concentration fluctuations in startup shear flow, and their relationship to the observed nonhomogeneous flow, *in situ* rheomicroscopy measurements were performed on the PS-DOP solutions. The $Z = 30$ PS-DOP fluid exhibits fluctuations in concentration shortly after initiation of shear (Fig. 8). The fluid is initially optically isotropic [Fig. 8(a), dark between cross polarizers], then becomes oriented along the flow direction [Figs. 8(b) and 8(c), bright], and finally becomes dark again at long times [Fig. 8(d), steady flow]. Applying a digital Fourier band pass filter emphasizes the presence of heterogeneities in the fluid indicated by optical turbidity by removing long wavelength illumination gradients while preserving the local structure of the birefringent texture. These heterogeneities first appear at the moving cylinder [Fig. 8(b)], and then propagate into the bulk [Fig. 8(c)]. At long times [Fig. 8(d)] the heterogeneities appear to subside. To further highlight the emergence and disappearance of strong flow-enhanced concentration fluctuations, we average the image intensity along the vertical (flow) direction (Fig. 8, bottom row). As apparent in Fig. 8(c), there is a periodicity to the contour profile. Based on the periodicity in the contour profile, it is estimated that the fluctuations are $8.5-9.5\,\mu$m,

slightly larger than results of lower molecular weight PS-DOP solutions [12,13,24,52]. We note that there is no discernible change of turbidity in the rheo-PTV images upon shearing the $Z = 16$ fluid at $T = 22\,^{\circ}\mathrm{C}$, where the inversely bowed velocity profiles are not observed, but we do observe changes in turbidity in the rheo-PTV images upon shearing the $Z = 30$ and 36 fluids at $T = 50\,^{\circ}\mathrm{C}$. These preliminary results suggest that inversely bowed velocity profiles do not occur in the absence of shear-enhanced turbidity.

Interestingly, we find a strong correlation between the observed regions of concentration heterogeneity and the local shear rate in these regions when nonhomogeneous velocity profiles develop (Fig. 9). Prior to the overshoot in shear stress, the velocity profile remains uniform and there are no apparent heterogeneities in the rheomicroscopy images [Fig. 9(a)]. Following the overshoot in the shear stress, the fluid develops noticeable optical heterogeneities that are spatially nonuniform [Fig. 9(b)]. The location of the heterogeneities, adjacent to the moving cylinder, coincides with the location and width of the low shear rate region as measured from rheo-PTV [Fig. 9(b)]. Finally, at long times, the presence of heterogeneities in the rheomicroscopy images subsides, and the velocity profile returns to a homogeneous shear rate. To rationalize this behavior, we suggest that flow-enhanced concentration heterogeneities increase the local "effective" fluid viscosity. In Taylor-Couette flow, the shear stress is highest at the inner moving cylinder and lowest at the stationary outer cylinder. By increasing the local fluid viscosity, the apparent shear rate must therefore decrease to maintain stress continuity across the fluid. These results suggest that the mechanism by which nonhomogeneous flow arises in the highly entangled PS-DOP solutions is closely related to, if not caused by, the appearance of local concentration fluctuations in the region of highest shear stress near the inner moving wall.

An obvious question, given the large changes in the velocity profiles, is whether the required changes in the apparent viscosity are "reasonable." The velocity gradient in the low shear rate region decreases by as much as a factor of 13 relative to the nominal imposed shear rate ($\dot{\gamma}_{\mathrm{app}}$), which might superficially suggest that concentration fluctuations correspond to an increase of the apparent viscosity of a similar magnitude. Although we do not have a theoretical means at this stage to estimate how much change the additional dissipation could generate, a factor of 13 would seem to be "unreasonable." However, it is important to recognize that the change in the velocity gradient in the low shear rate region is significantly amplified by strong shear thinning in the high shear rate region.

One way to see this is to calculate the local apparent viscosities in the high and low shear rate regions (Fig. 10). The local viscosity of the low shear rate region adjacent to the inner cylinder [$\eta^{+}_{\mathrm{inner}}(t)$] is given by

$$\eta^{+}_{\mathrm{inner}}(t) = \frac{\sigma_{\mathrm{inner}}(t)}{\dot{\gamma}_{\mathrm{inner}}(t)}. \tag{4}$$

Here $\dot{\gamma}_{\mathrm{inner}}(t)$ is the measured shear rate in the region adjacent to the inner cylinder as quantified from a linear regression of the velocity profile data over which an approximately constant velocity gradient is observed. $\sigma_{\mathrm{inner}}(t)$ represents a spatially averaged shear stress over the width of the low shear rate region, calculated by means of the known shear stress gradient in Taylor-Couette flow, given by

$$\sigma(r,t) = \sigma_{\mathrm{wall}}(t)\frac{R_i^2}{\left[\left(\frac{r}{H} + R_i\right)^2\right]}, \tag{5}$$

where $\sigma_{\mathrm{wall}}(t)$ is the shear stress measured by the rheometer.

Similarly, the local apparent viscosity of the outer region is calculated by

$$\eta^{+}_{\mathrm{outer}}(t) = \frac{\sigma_{\mathrm{outer}}(t)}{\dot{\gamma}_{\mathrm{outer}}(t)}. \tag{6}$$

Here $\dot{\gamma}_{\mathrm{outer}}$ is the measured shear rate adjacent to the outer cylinder as computed from a linear regression of the velocity profile in the high shear region over which an approximately constant

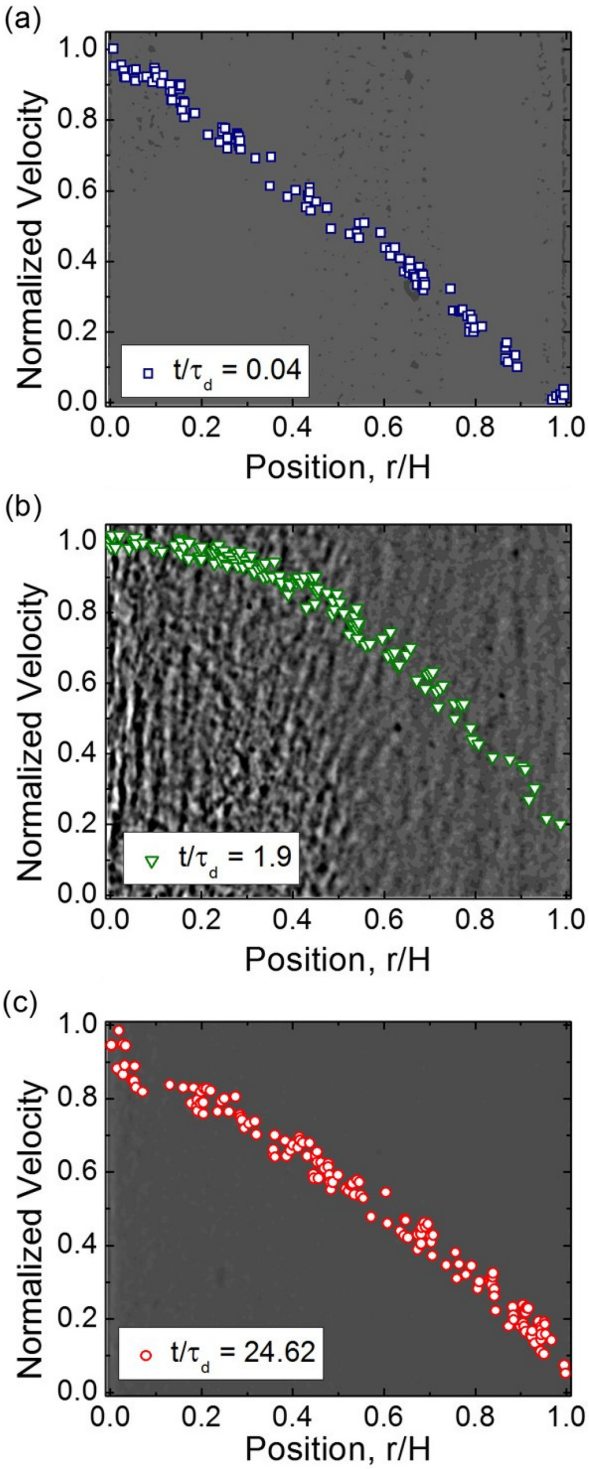

FIG. 9. Transient development of velocity profiles of 16 wt% PS(3.84M)-DOP at $Wi_{\text{app}} = 11.1$ overlaid on corresponding images collected in rheomicroscopy with a band pass filter applied showing shear-enhanced concentration fluctuations at (a) $\frac{t}{\tau_d} = 0.04$, (b) $\frac{t}{\tau_d} = 1.9$, and (c) $\frac{t}{\tau_d} = 24.62$.

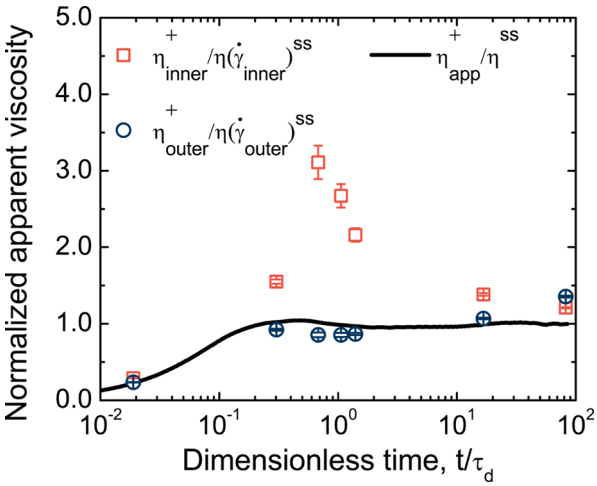

FIG. 10. Normalized transient viscosity as measured by the rheometer compared to spatially resolved apparent viscosities adjacent to the inner and outer cylinders of the Taylor-Couette geometry for 10 wt% PS(8.42M)-DOP at $Wi_{app} = 5.29$. The open symbols represent the local transient viscosities normalized by the steady state viscosities at the locally measured shear rates [$\eta(\dot{\gamma}_{inner})^{SS}$ and $\eta(\dot{\gamma}_{outer})^{SS}$]. The solid black line represents the measured transient viscosity at the nominal imposed shear rate normalized by the steady state viscosity.

velocity gradient is observed. $\sigma_{outer}(t)$ represents a spatially averaged shear stress over the width of the high shear rate region, calculated following the same procedure as for $\sigma_{inner}(t)$.

The results for η^+_{outer} and η^+_{inner} are plotted in Fig. 10, normalized by the measured steady state viscosity at the corresponding local shear rate, $\eta(\dot{\gamma}_{inner})^{SS}$ and $\eta(\dot{\gamma}_{outer})^{SS}$, respectively. These ratios, $\eta^+_{outer}/\eta(\dot{\gamma}_{outer})^{SS}$ and $\eta^+_{inner}/\eta(\dot{\gamma}_{inner})^{SS}$, quantify the deviation in the locally observed viscosity relative to the steady state due to the transient viscoelasticity of the fluid. This deviation includes any possible effects due to concentration fluctuations and concomitant nonhomogeneous flow.

We compare this quantity in Fig. 10 to the apparent transient viscosity determined from the measured wall shear stress, $\sigma_{wall}(t)$, and $\dot{\gamma}_{app}$,

$$\eta^+_{app}(t) = \frac{\sigma_{wall}(t)}{\dot{\gamma}_{app}}, \tag{7}$$

normalized by its steady state value, $\eta(\dot{\gamma}_{app})^{SS}$. This latter ratio, $\eta^+_{app}/\eta(\dot{\gamma}_{app})^{SS}$, represents the deviation of the apparent transient viscosity from its steady state value in the absence of any information about the velocity profile due to apparent viscoelastic effects. Given these definitions, it is then clear that any deviation of the locally observed viscosity ratios, $\eta^+_{inner}/\eta(\dot{\gamma}_{inner})^{SS}$ and $\eta^+_{outer}/\eta(\dot{\gamma}_{outer})^{SS}$, from the apparent viscosity ratio $\eta^+_{app}/\eta(\dot{\gamma}_{app})^{SS}$ are due solely to the effects of the nonhomogeneous velocity profile, which we have hypothesized as being due to the effects of concentration fluctuations (Fig. 10).

The value of $\eta^+_{outer}/\eta(\dot{\gamma}_{outer})^{SS}$ (open blue circles), in which the amplitude of transient concentration fluctuations remains small throughout the measurement, is consistent at all times with the measured steady state viscosity at the local shear rate in a homogeneous fluid (i.e., $\eta^+_{outer}/\eta(\dot{\gamma}_{outer})^{SS} \approx 1$) [62]. On the other hand, $\eta^+_{inner}/\eta(\dot{\gamma}_{inner})^{SS}$ (open red squares), in which the amplitude of shear-enhanced concentration fluctuations is large, is found to exceed the steady state viscosity by about a factor of 3. While a threefold enhancement of viscosity due to fluctuations in concentration still seems somewhat large, it is important to note that there are currently no theories capable of predicting how large of a change in viscosity the shear-enhanced concentration fluctuations could produce. As already stated, the fact that only a factor of 3 change in the apparent

viscosity is required to account for the observed changes in the velocity gradient in the low shear rate region is a consequence of the very significant reduction of the viscosity in the high shear rate region due to the effects of shear thinning.

IV. CONCLUSIONS

Rheo-PTV measurements of highly entangled polystyrene solutions reveal departures from uniform flow during startup shear that cannot be explained by the expected rheology of a homogeneous polymeric fluid. Despite these departures from the anticipated behavior, the transient and steady state shear stresses of all solutions investigated agree with Rolie-Poly model predictions and previously reported experiments. *In situ* rheomicroscopy measurements confirm the presence of shear-enhanced concentration fluctuations in the highly entangled fluids. Specifically, a spatial gradient in the magnitude of the concentration fluctuations is found to coincide with an inverse gradient in the local shear rate. This experimental observation suggests nonhomogeneous flows in entangled polymers can arise from a coupling of banded flows to local concentration fluctuations. Because the fluids we study are representative of a large body of near-critical polymer solutions, these findings call for deeper examination of the generality of this behavior to other material systems involving polymer solutions, and also potentially other fluids exhibiting coupling of thermal fluctuations and flow [63–68].

A possible explanation of this phenomenon is that the presence of concentration heterogeneities increases the local effective viscosity of the fluid through extra dissipation. Based on this proposed mechanism, we expect that the transient nonhomogeneous flows reported here should also occur in other situations where flow produces sufficiently strong spatial variations in the amplitude of concentration fluctuations. Recently developed rheological models involving the coupling of entangled polymer dynamics with nonlocal concentration fluctuations are a logical starting point for developing a full theoretical description of the phenomena we report [28,29]. However, due to the necessity for numerically resolving 3D spatiotemporally evolving concentration fields, we leave such investigations to future studies.

This work provides further support that nonhomogeneous flow can occur in startup shear of entangled polymer solutions even when potential experimental artifacts known to nonlinear rheology are accounted for, and it highlights the importance of considering fluid nonuniformities when interpreting the nonhomogeneous flow of polymeric fluids. It also calls for deeper fundamental studies into the influence of enhanced local concentration fluctuations on the rheology of polymer solutions, and the coupling of these effects to the underlying flow. Finally, we note that the findings of this work could have more general consequences involving the effects of flow-enhanced thermal fluctuations on other transport properties, as well as other fields that could be coupled with enhanced fluctuations.

ACKNOWLEDGMENTS

The authors would like to thank Dr. Y. Thomas Hu and Unilever for the donation of the Anton Paar MCR-300 rheometer fitted with the optics necessary for the rheo-PTV measurements. In addition, the authors are grateful for the use of an Anton Paar MCR-702 rheometer for the rheomicroscopy measurements made possible by the Anton Paar VIP program. This work was supported by the National Science Foundation under Award No. CBET-1510333. Partial support for MCB was provide by the National Science Foundation under Award No. CBET-1729108.

[1] M. Doi and S. F. Edwards, Dynamics of concentrated polymer systems: Part III—The constitutive equation, J. Chem. Soc., Faraday Trans. 2 **74**, 1818 (1978).

[2] P. G. De Gennes, Reptation of a polymer chain in the presence of fixed obstacles, J. Chem. Phys. **55**, 572 (1971).
[3] D. W. Mead, R. G. Larson, and M. Doi, A molecular theory for fast flows of entangled polymers, Macromolecules **31**, 7895 (1998).
[4] Y. T. Hu, L. Wilen, A. Philips, and A. Lips, Is the constitutive relation for entangled polymers monotonic? J. Rheol. **51**, 275 (2007).
[5] S. T. Milner, T. C. B. McLeish, and A. E. Likhtman, Microscopic theory of convective constraint release, J. Rheol. **45**, 539 (2001).
[6] R. S. Graham, A. E. Likhtman, T. C. B. McLeish, and S. T. Milner, Microscopic theory of linear, entangled polymer chains under rapid deformation including chain stretch and convective constraint release, J. Rheol. **47**, 1171 (2003).
[7] E. V. Menezes and W. W. Graessley, Nonlinear rheological behavior of polymer systems for several shear-flow histories, J. Polym. Sci. Part B: Polym. Phys. **20**, 1817 (1982).
[8] A. E. Likhtman and R. S. Graham, Simple constitutive equation for linear polymer melts derived from molecular theory: Rolie-Poly equation, J. Non-Newtonian Fluid Mech. **114**, 1 (2003).
[9] S. Costanzo, Q. Huang, G. Ianniruberto, G. Marrucci, O. Hassager, and D. Vlassopoulos, Shear and extensional rheology of polystyrene melts and solutions with the same number of entanglements, Macromolecules **49**, 3925 (2016).
[10] C. Rangel-Nafaile, A. B. Metzner, and K. F. Wissbrun, Analysis of stress-induced phase separations in polymer solutions, Macromolecules **17**, 1187 (1984).
[11] T. Kume, T. Hashimoto, T. Takahashi, and G. G. Fuller, Rheo-optical studies of shear-induced structures in semidilute polystyrene solutions, Macromolecules **30**, 7232 (1997).
[12] X. L. Wu, D. J. Pine, and P. K. Dixon, Enhanced Concentration Fluctuations in Polymer Solutions under Shear Flow, Phys. Rev. Lett. **66**, 2408 (1991).
[13] P. K. Dixon, D. J. Pine, and X. L. Wu, Mode Selection in the Dynamics of Sheared Polymer Solutions, Phys. Rev. Lett. **68**, 2239 (1992).
[14] E. Helfand and G. H. Fredrickson, Large Fluctuations in Polymer Solution under Shear, Phys. Rev. Lett. **62**, 2468 (1989).
[15] J. W. van Egmond, D. E. Werner, and G. G. Fuller, Time-dependent small-angle light scattering of shear-induced concentration fluctuations in polymer solutions, J. Chem. Phys. **96**, 7742 (1992).
[16] T. Hashimoto and K. Fujioka, Shear-enhanced concentration fluctuations in polymer solutions as observed by flow light scattering, J. Phys. Soc. Jpn. **60**, 356 (1991).
[17] S. Saito, T. Hashimoto, I. Morfin, P. Lindner, and F. Boué, Structures in a semidilute polymer solution induced under steady shear flow as studied by small-angle light and neutron scattering, Macromolecules **35**, 445 (2002).
[18] M. K. Endoh, S. Saito, and T. Hashimoto, Shear-induced structures in semidilute polystyrene solution: Effect of solvent quality, Macromolecules **35**, 7692 (2002).
[19] S. Saito, T. Hashimoto, I. Morfin, P. Lindner, F. Boué, and D. J. Pine, Phase separation in a polymer solution induced by steady and large amplitude oscillatory shear flow, Macromolecules **36**, 3745 (2003).
[20] L. Hilliou and D. Vlassopoulos, Time-periodic structures and instabilities in shear-thickening, Ind. Eng. Chem. Res. **41**, 6246 (2002).
[21] M. K. Endoh, M. Takenaka, T. Inoue, H. Watanabe, and T. Hashimoto, Shear small-angle light scattering studies of shear-induced concentration fluctuations and steady state viscoelastic properties, J. Chem. Phys. **128**, 164911 (2008).
[22] P. Moldenaers, H. Yanase, J. Mewis, G. G. Fuller, C.-S. Lee, and J. J. Magda, Flow-induced concentration fluctuations in polymer solutions: Structure/property relationships, Rheol. Acta **32**, 1 (1993).
[23] T. Kume, T. Hattori, and T. Hashimoto, Time evolution of shear-induced structures in semidilute polystyrene solutions, Macromolecules **30**, 427 (1997).
[24] K. Migler, C. H. Liu, and D. J. Pine, Structure evolution of a polymer solution at high shear rates, Macromolecules **29**, 1422 (1996).
[25] H. Yanase, P. Moldenaers, J. Mewis, V. Abetz, J. van Egmond, and G. G. Fuller, Structure and dynamics of a polymer solution subject to flow-induced phase separation, Rheol. Acta **30**, 89 (1991).

[26] S. Saito, K. Matsuzaka, and T. Hashimoto, Structures of a semidilute polymer solution under oscillatory shear flow, Macromolecules **32**, 4879 (1999).
[27] M. Cromer, M. C. Villet, G. H. Fredrickson, and L. G. Leal, Shear banding in polymer solutions, Phys. Fluids **25**, 051703 (2013).
[28] M. Cromer, G. H. Fredrickson, and L. G. Leal, A study of shear banding in polymer solutions, Phys. Fluids **26**, 063101 (2014).
[29] J. D. Peterson, M. Cromer, G. H. Fredrickson, and L. G. Leal, Shear banding predictions for the two-fluid Rolie-Poly model, J. Rheol. **60**, 927 (2016).
[30] S. M. Fielding and P. D. Olmsted, Flow phase diagrams for concentration-coupled shear banding, Eur. Phys. J. E **11**, 65 (2003).
[31] S. M. Fielding and P. D. Olmsted, Early Stage Kinetics in a Unified Model of Shear-Induced Demixing and Mechanical Shear Banding Instabilities, Phys. Rev. Lett. **90**, 224501 (2003).
[32] S. M. Fielding and P. D. Olmsted, Kinetics of the shear banding instability in startup flows, Phys. Rev. E **68**, 036313 (2003).
[33] S. Ravindranath, S.-Q. Wang, M. Olechnowicz, and R. P. Quirk, Banding in simple steady shear of entangled polymer solutions, Macromolecules **41**, 2663 (2008).
[34] P. E. Boukany, S.-Q. Wang, S. Ravindranath, and L. J. Lee, Shear banding in entangled polymer in the micron scale gap: A confocal-rheoscopic study, Soft Matter **11**, 8058 (2015).
[35] S. Cheng and S.-Q. Wang, Is shear banding a metastable property of well-entangled polymer solutions? J. Rheol. **56**, 1413 (2012).
[36] S. Jaradat, M. Harvey, and T. A. Waigh, Shear-banding in polyacrylamide solutions revealed via optical coherence tomography velocimetry, Soft Matter **8**, 11677 (2012).
[37] Y. T. Hu, Steady-state shear banding in entangled polymers? J. Rheol. **54**, 1307 (2010).
[38] S. Shin, K. D. Dorfman, and X. Cheng, Shear-banding and superdiffusivity in entangled polymer solutions, Phys. Rev. E **96**, 062503 (2017).
[39] S. Shin, K. D. Dorfman, and X. Cheng, Effect of edge disturbance on shear banding in polymeric solutions, J. Rheol. **62**, 1339 (2018).
[40] P. Cheng, M. C. Burroughs, L. G. Leal, and M. E. Helgeson, Distinguishing shear banding from shear thinning in flows with a shear stress gradient, Rheol. Acta **56**, 1007 (2017).
[41] Y. Li, M. Hu, G. B. McKenna, C. J. Dimitriou, G. H. McKinley, R. M. Mick, D. C. Venerus, and L. A. Archer, Flow field visualization of entangled polybutadiene solutions under nonlinear viscoelastic flow conditions, J. Rheol. **57**, 1411 (2013).
[42] Y. Li and G. B. McKenna, Startup shear of a highly entangled polystyrene solution deep into the nonlinear viscoelastic regime, Rheol. Acta **54**, 771 (2015).
[43] C. Sui and G. B. McKenna, Instability of entangled polymers in cone and plate rheometry, Rheol. Acta **46**, 877 (2007).
[44] Y. W. Inn, K. F. Wissbrun, and M. M. Denn, Effect of edge fracture on constant torque rheometry of entangled polymer solutions, Macromolecules **38**, 9385 (2005).
[45] J. M. Adams and P. D. Olmsted, Nonmonotonic Models are Not Necessary to Obtain Shear Banding Phenomena in Entangled Polymer Solutions, Phys. Rev. Lett. **102**, 067801 (2009).
[46] S. Ravindranath and S.-Q. Wang, Steady state measurements in stress plateau region of entangled polymer solutions: Controlled-rate and controlled-stress modes, J. Rheol. **52**, 957 (2008).
[47] S. T. Milner, Dynamical theory of concentration fluctuations in polymer solutions under shear, Phys. Rev. E **48**, 3674 (1993).
[48] H. Ji and E. Helfand, Concentration fluctuations in sheared polymer solutions, Macromolecules **28**, 3869 (1995).
[49] A. Onuki, Dynamic equations of polymers with deformations in semidilute regions, J. Phys. Soc. Jpn. **59**, 3423 (1990).
[50] H. Murase, T. Kume, T. Hashimoto, and Y. Ohta, Shear-induced structures in semidilute solution of ultrahigh molecular weight polyethylene at temperature close to equilibrium dissolution temperature, Macromolecules **38**, 6656 (2005).

[51] M. K. Endoh, M. Takenaka, and T. Hashimoto, Effects of shear flow on a semidilute polymer solution under phase-separating condition, Polymer **47**, 7271 (2006).
[52] E. Moses, T. Kume, and T. Hashimoto, Shear Microscopy of the "Butterfly Pattern" in Polymer Mixtures, Phys. Rev. Lett. **72**, 2037 (1994).
[53] V. R. Mhetar and L. A. Archer, Slip in entangled polymer solutions, Macromolecules **31**, 8617 (1998).
[54] Y. T. Hu and A. Lips, Kinetics and mechanism of shear banding in an entangled micellar solution, J. Rheol. **49**, 1001 (2005).
[55] J. Crocker and D. Grier, Methods of digital video microscopy for colloidal studies, J. Colloid Interface Sci. **179**, 298 (1996).
[56] R. G. Larson, E. S. G. Shaqfeh, and S. J. Muller, A purely elastic instability in Taylor-Couette flow, J. Fluid Mech. **218**, 573 (1990).
[57] See Supplemental Material at http://link.aps.org/supplemental/10.1103/PhysRevFluids.5.043301 for details about the homogeneous Rolie-Poly model formulation, complications of nonlinear rheology measurements in entangled polymer solutions, effect of Deborah number on the observed velocity profiles, and shear-enhanced concentration fluctuations observed in rheomicroscopy, which contains Refs. [69–74].
[58] T. Inoue, Y. Yamashita, H. Watanabe, M. K. Endoh, and T. Hashimoto, Stress overshoot of entangled polymers in Θ solvent, Macromolecules **37**, 4317 (2004).
[59] S. Mani, M. F. Malone, and H. H. Winter, Shear-induced demixing in a polystyrene/poly (vinyl methyl ether) blend: In-situ fluorescence and rheometry, Macromolecules **25**, 5671 (1992).
[60] R. G. Larson, Flow-induced mixing, demixing, and phase transitions in polymeric fluids, Rheol. Acta **31**, 497 (1992).
[61] J. J. Magda, C. S. Lee, S. J. Muller, and R. G. Larson, Rheology, flow instabilities, and shear-induced diffusion in polystyrene solutions, Macromolecules **26**, 1696 (1993).
[62] Of course, this value (η^+_{outer}) is as small as ∼25% of the apparent measured transient viscosity (η^+_{app}), due to shear thinning.
[63] J. F. Le Meins and J. F. Tassin, Shear-induced phase separation in an associating polymer solution, Macromolecules **34**, 2641 (2001).
[64] P. Boltenhagen, Y. Hu, E. F. Matthys, and D. J. Pine, Observation of Bulk Phase Separation and Coexistence in a Sheared Micellar Solution, Phys. Rev. Lett. **79**, 2359 (1997).
[65] B. A. Schubert, N. J. Wagner, E. W. Kaler, and S. R. Raghavan, Shear-induced phase separation in solutions of wormlike micelles, Langmuir **20**, 3564 (2004).
[66] P. Thareja, I. H. Hoffmann, M. W. Liberatore, M. E. Helgeson, Y. T. Hu, M. Gradzielski, and N. J. Wagner, Shear-induced phase separation (SIPS) with shear banding in solutions of cationic surfactant and salt, J. Rheol. **55**, 1375 (2011).
[67] B. Belzung, F. Lequeux, J. Vermant, and J. Mewis, Flow-induced anisotropy in mixtures of associative polymers and latex particles, J. Colloid Interface Sci. **224**, 179 (2000).
[68] M. W. Liberatore, N. B. Wyatt, M. Henry, P. L. Dubin, and E. Foun, Shear-induced phase separation in polyelectrolyte/mixed micelle coacervates, Langmuir **25**, 13376 (2009).
[69] S. Q. Wang, G. Liu, S. Cheng, P. E. Boukany, Y. Wang, and X. Li, Letter to the Editor: Sufficiently entangled polymers do show shear strain localization at high enough Weissenberg numbers, J. Rheol. **58**, 1059 (2014).
[70] E. J. Hemingway, H. Kusumaatmaja, and S. M. Fielding, Edge Fracture in Complex Fluids, Phys. Rev. Lett. **119**, 028006 (2017).
[71] J. Sanchez-Reyes and L. A. Archer, Steady shear rheology of entangled polymer liquids: Implications of interfacial slip, J. Rheol. **46**, 1239 (2002).
[72] J. Sanchez-Reyes and L. A. Archer, Interfacial slip violations in polymer solutions: Role of microscale surface roughness, Langmuir **19**, 3304 (2003).
[73] F. Brochard and P. G. de Gennes, Shear-dependent slippage at a polymer/solid interface, Langmuir **8**, 3033 (1992).
[74] H. Müller-Mohnssen, D. Weiss, and A. Tippe, Concentration dependent changes of apparent slip in polymer solution flow, J. Rheol. **34**, 223 (1990).